RSC Advances

ROYAL SOCIETY OF CHEMISTRY

www.rsc.org/advances

Corrosion inhibition of functional graphene reinforced polyurethane nanocomposite coatings with regular texture

Mengting Mo[a,b], Wenjie Zhao[a,1], Zifei Chen[a,b], Eryong Liu[a], Qunji Xue[a]

[a] *Key Laboratory of Marine Materials and Related Technologies, Zhejiang Key Laboratory of Marine Materials and Protective Technologies, Ningbo Institute of Materials Technology and Engineering, Chinese Academy of Sciences, Ningbo 315201, P.R. China*

[b] *University of Chinese Academy of Sciences, Beijing, 100049, P.R. China*

ABSTRACT:

In order to further enhance its anti-corrosion properties as surface coatings for protecting various materials from corrosion, polyurethane (PU) needs to be modified via adjusting chemical composition and interface structure. In this work, a series of functionalized graphene (FG) reinforced PU nanocomposite coatings with regular texture were fabricated using replication method. The structural and morphological properties of as-prepared PU composite coatings were characterized by Fourier transform infrared spectroscopy, Raman spectroscopy, X-ray photoelectron spectrometer, transmission electron microscopy, scanning electron microscopy and atomic force microscopy. Results showed that FG was dispersed homogeneously in the PU matrix after chemical modification. Moreover, the morphology of the obtained coatings showed circular cone with a diameter of 8 μm spaced 8, 6 and 4 μm apart, respectively. Most important, the presence of surface texture and well-dispersed FG effectively enhanced the anti-corrosion properties of textured FG/PU composite coating. It is attributed to the hydrophobicity and barrier effect of the obtained coatings, which not only reduce the contact and interaction between water and surfaces, but also increase the tortuosity of corrosive medium diffusion pathway.

Keywords: polyurethane nanocomposite coatings, graphene, texture, synergistic effect, anti-corrosion

1. Introduction

Majority of economy industries are confronted with the costly problem of corrosion under various environmental conditions, which is a serious constraint to working efficiency and

[1] Corresponding author. Tel: +86-0574-86694901.
E-mail address: zhaowj@nimte.ac.cn (W. J. Zhao).

mechanical durability of the equipment. Therefore, corrosion protection is extremely important and necessary in almost all the fields such as marine, pipeline, aerospace, automobiles and construction industries[1]. However, corrosion can't be completely prevented, and thus, corrosion control strategies concentrate on delaying the corrosion process and altering the corrosion mechanism[2, 3]. Organic protective coatings, such as epoxy resin, acrylic easter and polyurethane (PU) etc., have been employed as the most convenient and widely used one to protect materials against corrosion [4].

PU is characterized as the typical urethane functional group (-NHCO-O-), which is usually formed by reaction between isocyanate and hydroxyl groups from polyisocyanates and polyols[5, 6]. PU has been widely used in manufacture industry, daily life, health care, and even the national defense industry due to a variety of advantages, such as outstanding abrasion resistance, corrosion resistance, excellent flexibility, strong adhesion to substrates, possibility of tailoring properties, and also some other specific [7-10]. Whereas, its shortcomings, such as unsatisfactory thermal stability, stiffness, tensile strength and barrier properties, restrict its extensive applications[11, 12]. As a consequence, PU needs to be modified to further enhance its anti-corrosion properties as surface coatings for protecting various materials from corrosion.

Recently, graphene (G) have emerged as a promising building block used in polymer matrix on account of its unique geometry and novel physical properties, such as ultrahigh specific surface area (2600 m2/g),superior mechanical strength (Young's modulus to 1060 GPa), high aspect ratio, electrical mobility (200000 ccm2/(V·s)) and thermal conductivity (5000W/(mK)), barrier properties and low raw material cost [13-20]. In particular, as reported in previous literatures, G has a giant application potential in corrosion protection fields. Chang et al.[21] reported that G provide a more desirable anticorrosion properties for polyaniline than clay resulted from having higher aspect ratio. Chang et al.[22] stated that the well-dispersed G displayed remarkable anti-corrosion properties because of enhanced barrier properties.

Unfortunately, the presence of strong intrinsic van der Waals attraction between the fillers and the absence of bond between G and the polymer matrix, pose a substantial obstacle to get graphene-based composites with excellent dispersion and compatibility. To a great extent, this impairs anti-corrosion performance of the graphene-based composites. In order to figure out the problem, the most common and convenient strategy is chemical modification, including covalent[18,

[23-26] and non-covalent[27-30] manner. The chemical modification of graphene not only greatly weakens the intermolecular interactions which can prevent the stack and agglomerate of fillers to improve its solubility and dispersion, but also enhances the interfacial interaction between polymer matrix and G through covalent linkage or non-covalent bonding (such as hydrogen bonding and electrostatic interactions) [10, 18, 31]. In addition, it is generally known that a variety of siloxane coupling agents have been widely used to the chemical modification of G via the chemical reaction between the trialkoxy groups of siloxane coupling agent and the hydroxyl groups of G. Previous studies[11, 12] have shown that the covalent functionalization of G could improve both the dispersion of G in the polymer matrix and the interfacial interactions between G and polymer matrix. Meanwhile, it provided a simple method to fabricate nanocomposite coatings with effectively enhanced thermal and mechanical properties.

Meanwhile, researchers have realized that surface texture has great signification for enhancing the anti-corrosion properties of materials, and various studies have been carried out so far in this field. de Leon et al.[2] fabricated a series of superhydrophobic textured polythiophene coatings, which has been proven to display excellent corrosion protection capability. Chang et al.[34] prepared composite coatings with a hydrophobic surface of the biomimetic natural leaf, and found that the hydrophobicity and barrier effect of the obtained materials provided them with excellent anticorrosive properties. To sum up the results of research work, surface texture provided materials with better hydrophobic property, and thus influencing the anti-corrosion properties[2, 35]. To be specific, a hydrophobic surface can reduce the contact and interaction between water and surfaces, and slowing the kinetics of the corrosion process[4, 36, 37]. Therefore, surface texture is considered as a promising method for improving anti-corrosion performance.

To the best of our knowledge, many studies have been previously carried out about the independent effect of nanofiller and surface texture on the anti-corrosion properties. However, utilizing the synergistic effect of nanofiller and textured surface (especially the regular textured surfaces) to prepare the anti-corrosion coatings, were rarely referred to. In particular, it is necessary to explore the relationship between texture density and anti-corrosion properties. In our previous studies, we studied tribological and anti-corrosion comprehensive behaviours of PU nanocomposite coatings, and the different functions served by G and graphene oxide (GO) as building block. Previous studies indicated that appropriate concentration of G can significantly

enhance the anti-corrosion properties of PU nanocomposite coatings. In our work, functionalized graphene (FG) was successfully synthesized by treating graphene with 3-aminopropyltriethoxysilane (APTES). Taking advantage of well dispersed FG and surface texture, a series of regular textured FG/PU composite coatings with different texture density were prepared. Fourier transform infrared spectroscopy (FT-IR), Raman spectroscopy and X-ray photoelectron spectrometer (XPS) were used to characterize the structural properties. Moreover, transmission electron microscopy (TEM), atomic force microscopy (AFM) and scanning electron microscopy (SEM) were performed to observe the morphological properties. Furthermore, wettability and anti-corrosion behaviours were studied comparatively by contact angle meter and electrochemical workstation. Finally, synergistic anti-corrosion mechanisms of textured FG/PU composite coatings were analyzed based on the experimental results.

2. Experimental

2.1. Materials

Hydroxyl acrylic resin (HAR: hydroxyl value=58 mg KOH/g) was supplied by Innotek TECHNOLOGY Co.,Ltd., China, and was diluted by dimethylbenzene (DMB, purchased from Aladdin Co.,Ltd., China). The curing agent hexamethylene diisocyanate (HMDI: NCO%=19.6%) was purchased from BAYER Co.,Ltd., German. G was purchased from Morsh Co.,Ltd., Ningbo, China. Ethanol, acetone, and silane coupling agent 3-aminopropyltriethoxysilane (APTES) were all produced by Sinopharm Chemical Reagent Co.,Ltd., China. The polydimethylsiloxane (PDMS) elastomer (SYLGARD® 184) was purchased from Dow Corning Co.,Ltd., china, and used as the masterplate material for texture formation due to its high reproducibility and good elasticity. All materials were used as received without further purification.

2.2. Preparation of PDMS template

Initially, regular textured silicon surfaces with different geometrical parameters were successfully prepared using inductively coupled plasma (ICP) etching technology[38]. Then, mix up nine parts by weight of SYLGARD® 184 resin with one part by weight SYLGARD® 184 curing agent. Next, the fabricated mixture was fully mixed with glass rod for 5 min, and air bubbles were removed under vacuum at room temperature for 10 min. Subsequently, the mixture was evenly

coated on the surface of textured wafers with appropriate thickness, and heat treated at 70 ℃ for 3 h. Finally, the PDMS elastomer was peel off from the textured wafers and used as template for imprinting.

2.3. Chemical modification of G

The synthesis process of FG was as follows: 2g of APTES, 0.8g of distilled water and 7.2g of alcohol were introduced into the beaker equipped with stirring for 10 min, then 0.1 g of G was added with ultrasonication for 1 h. Next, the suspension obtained was loaded into a round-bottom flask. The reaction was maintained for 6 h at 60 ℃ in a oil bath equipped with magnetic stirring. Finally, the slurry reaction mixture was centrifuged with 8000rmp for 8min and washed with ethanol and distilled water to remove residual APTES and achieve neutral, and then freeze-dried.

2.4. Preparation of textured FG/PU composite coatings

A series of regular textured FG/PU composite coatings with different texture density were prepared as follows: first of all, 0.03 g of FG was dispersed in ethanol with ultrasonic treatment for 30 min. Then 6 g of HAR was added into the above suspension with stirring for 1 h. Next, residual ethanol was removed carefully by stoving. Afterwards, the mixture was diluted by 2 g of DMB with stirring for 5 min, and then 1.62 g of HMDI was added as curing agent with stirring for 5 min. Subsequently, the mixture was degassed for 10 min under vacuum at room temperature, periodically breaking the vacuum to rupture the bubbles formed. After that, the mixture was coated on the surface of pretreatmented substrates (cast iron, polished by 800 mesh of sandpaper and then rinsed by ethanol ahead of time) by a wire bar coater with a thickness of 200 μm and 25 μm, respectively. Finally, cover the PDMS template on the surface of the FG/PU composite coatings for 3 h at 70 ℃, and then textured FG/PU composite coatings were obtained after peeling of the PDMS templates. The preparation process for textured FG/PU composite coatings is schematically illustrated in **Fig. 1**.

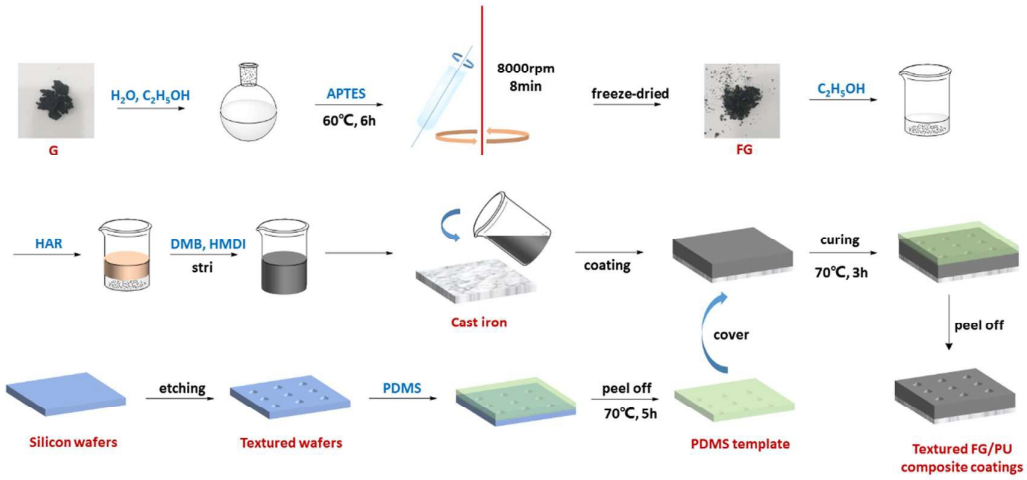

Fig. 1 Schematic illustration of the preparation process for textured FG/PU composite coatings

2.5. Characterization

The completion of chemical modification and curing was identified by FTIR (Nicolet 6700, Thermo Fisher Scientific, USA) in the 4000~500cm^{-1} scanning ranges.

The ordered and disordered crystal structures of filler before and after chemical modification were analyzed by Raman spectroscopy (Renishaw inVia Reflex, Renishaw, UK).

The chemical construction changes of components were characterized by XPS (Axis Utltra Dld, Shimadzu, Japan).

The morphology of the nanofiller and coatings was observed by TEM (JEM2100, JEOL, Japan).

The surface topography of textured wafers and textured FG/PU composite coatings was investigated by AFM (Agilent 5500, Agilent, USA) and SEM (FEI Quanta FEG 250, FEI, USA).

The surface water contact angle (WCA) of the samples was measured with a contact angle meter (OCA20, Dataphysics, Germany). The values of water contact angle were averages of five readings at different locations on each sample surface.

The anti-corrosion behaviours were characterized using an electrochemical workstation (Modulab, Solartron, UK) by potentiodynamic measurement in a three-electrode system: the sample, a platinum and a saturated calomel were used as the working, counter and reference electrode, perspectively. And the test area is confined to 0.2 cm^2. Prior to electrochemical tests, the testing section of working electrodes should be immersed in 3.5 wt% NaCl solution for 24h.

Potentiodynamic measurement of polarization curves in a Tafel model was conducted relative to the open circuit potential (OCP) within the potential range from -0.5 to 1 V vs at a scanning rate of 2 mV s^{-1}. Electrochemical impedance spectroscopic (EIS) measurements were carried out within the frequency ranging from 0.1 Hz to 10 kHz with a excitation amplitude of 10 mV.

3. Results and discussion

3.1. Structural properties

FTIR spectra of G, APTES, FG, HAR, HMDI and PU are presented in **Fig. 2**, which was compared to comfirm the successful completion of chemical modification and curing. The characteristic features of G included the characteristic absorption band corresponding to the OH stretching vibration at 3430 cm^{-1}, the C=C skeletal vibration from benzene ring structure at 1625 cm^{-1}, and the C–O–C stretching at 1056 cm^{-1}, respectively[18]. After reaction with APTES, new absorption peaks appeard at 1125 and 1030 cm^{-1} corresponding to absorption peak of Si-O-Si and C-O-Si group[39]. Meanwhile, the characteristic doublet at 2937 and 2860 cm^{-1} is ascribed to symmetric and asymmetric vibrations of the $–CH_2–$ group[40]. Moreover, it can't be ignored that the adsorption peak at 2970 and 1450 cm^{-1} corresponding to $–CH_3$ group from APTES was not observed in spectra of FG. All these changes of functional groups indicate that APTES is successfully bond to the surface of G. In addition, the characteristic absorption band at 3530 and 2270 cm^{-1} is ascribed to OH characteristic functional group from HAR and N=C=O group from HMDI, respectively[7, 41]. After condensation reaction, PU displays characteristic absorption at 1725 cm^{-1} corresponding to C=O stretching, and the the appearance of bands at 3358 cm^{-1} and 1533 cm^{-1} is attributed to the characteristic absorption of N-H groups[5, 42]. These characteristic absorption peaks demonstrate that PU is successfully synthesized by condensation reaction between OH group from HAR and N=C=O group from HMDI.

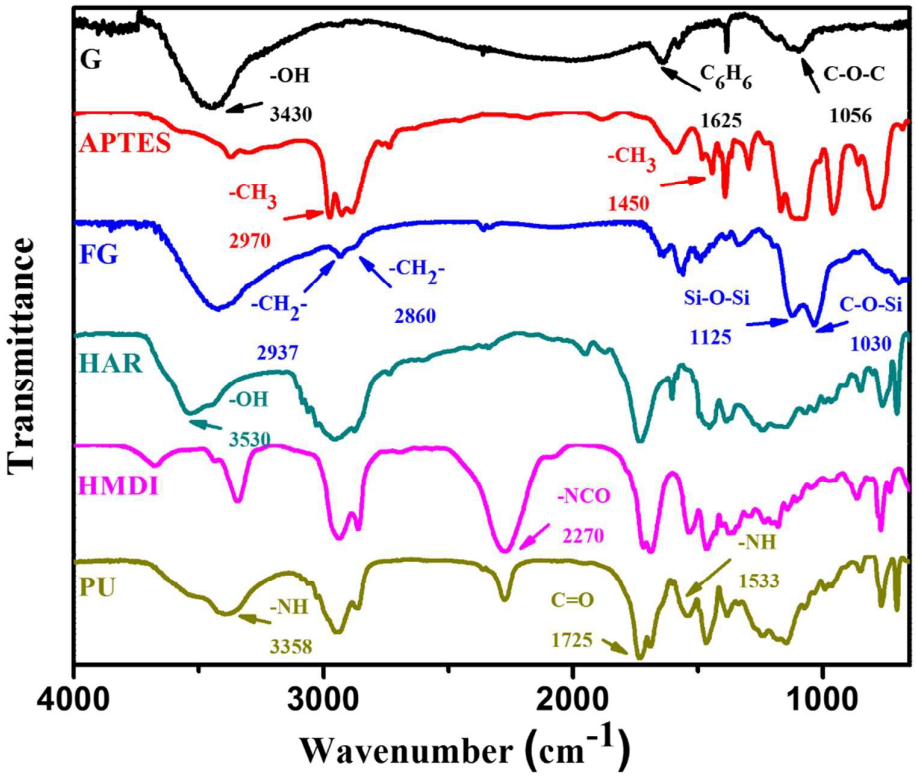

Fig. 2 FTIR spectra of G, APTES, FG, HAR, HMDI and PU

The changes of ordered and disordered crystal structures in G before and after chemical modification were characterized by Raman spectra. As shown in **Fig. 3**, both of G and FG exhibits an intense band (G) at 1580 cm^{-1}, which is attributed to the bond stretching of all atom pairs in both rings and chains in graphitic lattice (sp^2 carbon structure). Meanwhile, FG also displays a broad band (D) at 1350 cm^{-1} corresponding to defects in the graphitic domain[43]. In contrast, before chemical modification, little signal at the D band was observed, which indicates a low defect density of G. It is that contrast which not only illustrates the small amount of defects at the edge of graphene sheets, but also proved that the defects obviously increased due to the attachment of APTES. In addition, the intensity ratio of D and G (I_D/I_G) is a commonly used qualitative measure of defect density to probe the degree of graphitization[44]. The calculated result showed that I_D/I_G value of FG was 0.207, far higher than that of G (0.090). This also implies the surface oxygenic functional groups of G was successfully grafted with APTES.

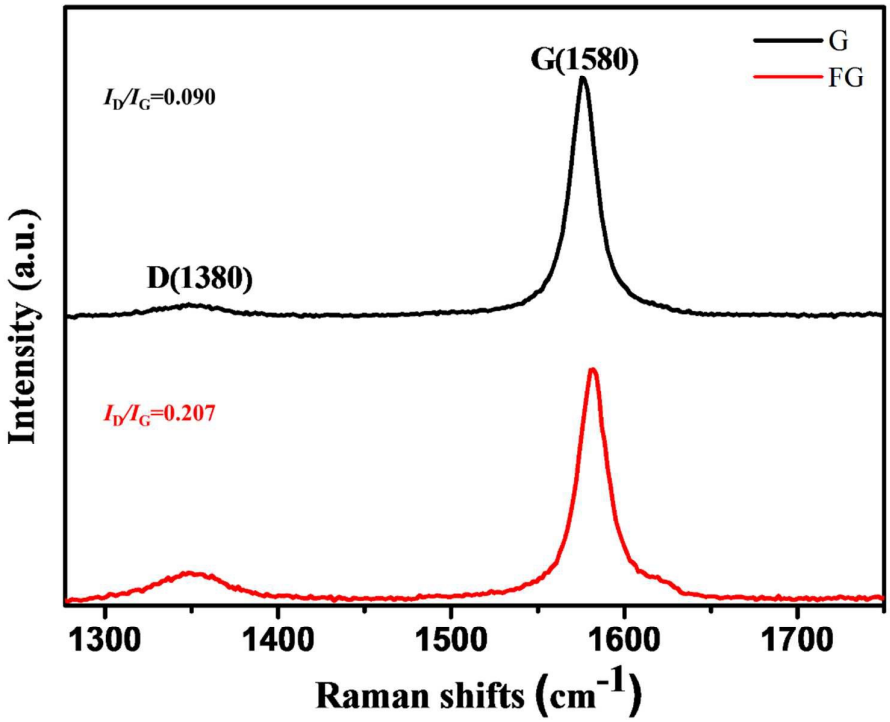

Fig. 3 Raman spectra of G and FG

FTIR and Raman results were further comfirmed by XPS analysis in **Fig. 4**, which display the C1s peak of G and PU, full XPS spectra and Si2p peak of G, FG, PU, FG/PU. As shown in **Fig. 4(a)**, the C1s peak of G can be deconvoluted into six components corresponding to carbon atoms in different functional groups including C-C (284.7eV), graphite (285.0eV), C-O (286.7 eV), C=O (287.6eV), O-C=O (288.9eV), $\pi - \pi^*$ (291.0 eV). When it comes to PU, its C1s XPS spectra in **Fig. 4(b)** shows four resolved peaks appearing at 284.7, 285.4, 286.7 and 288.9 eV, attributing to the functional groups of C-C, C-N, C-O and O–C=O. It further illustrates the condensation reaction between HAR and HMDI. As can be seen from **Fig. 4(c)**, the full XPS spectra of G, FG, PU and FG/PU presents four peaks including O1s, N1s, C1s and Si2p peak at 533, 400, 285 and 102 eV, respectively. Meanwhile, **Fig. 4(d)** is the Si2p spectra of G, FG, PU and FG/PU, which gives a single peak at 102 eV due to the presence of Si-O-C. Compared to G, the XPS spectra of FG shows an obvious increase in the O1s, N1s and Si 2p peaks. Likewise, a higher binding energy in the Si 2p peak can be observed in XPS spectra of FG/PU compared with that of PU. The above results sufficiently demonstrate the successful chemical modification of G and curing of PU[18, 40].

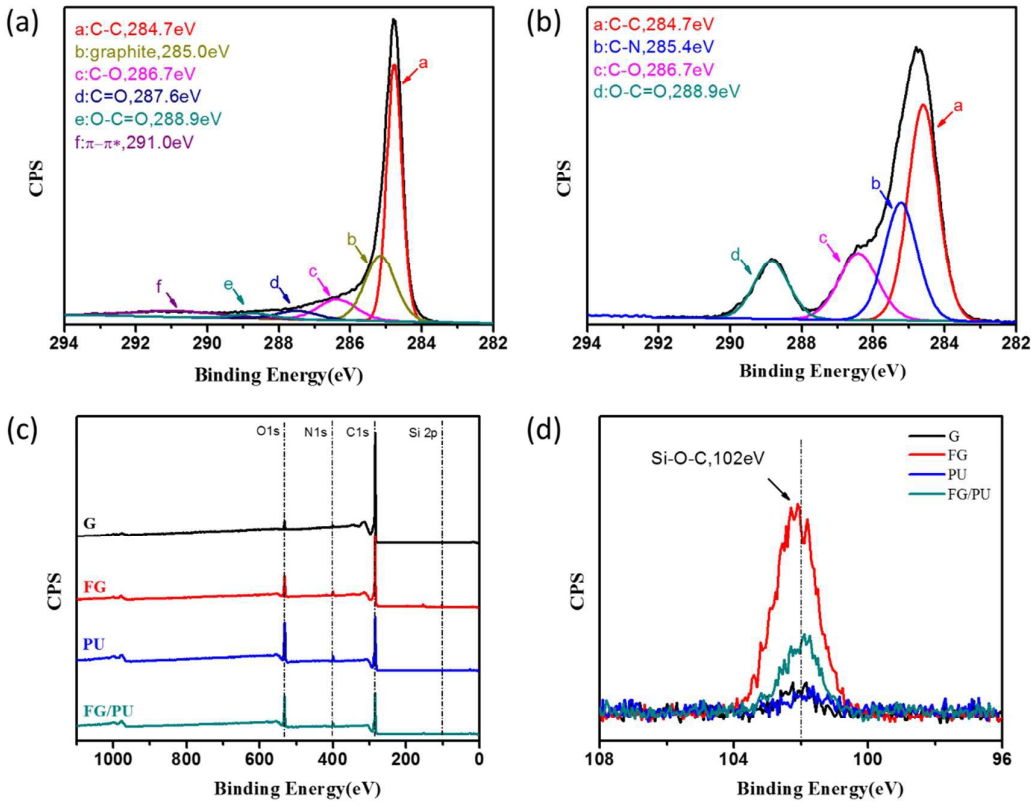

Fig. 4 C1s peak of G (a), PU (b), full XPS spectra (c) and Si2p peak (d) of G, FG, PU, FG/PU

3.2. Morphological properties

TEM observations shown in **Fig. 5** were performed to identify the nanoscopic dispersion state of G in ethanol and PU matrix. As shown in **Fig. 5(a)**, G exhibited a typically transparent and flat nanoplatelet shape, and the edges folded slightly[9, 45]. After chemical modification, partial region of FG in **Fig. 5(b)** seemed to be the dark contrast frequently attributing to the grafting silane at the plane and edge of G[40]. In addition, it can be observed in **Fig. 5(c)** that pure PU displayed uniform without any impurities. Meanwhile, FG presented in **Fig. 5(d)** was dispersed homogeneously in the PU matrix as folded nanosheet rather than caused agglomeration. The good dispersibility and compatibility of FG will provide a solid base for making the best of its own performance.

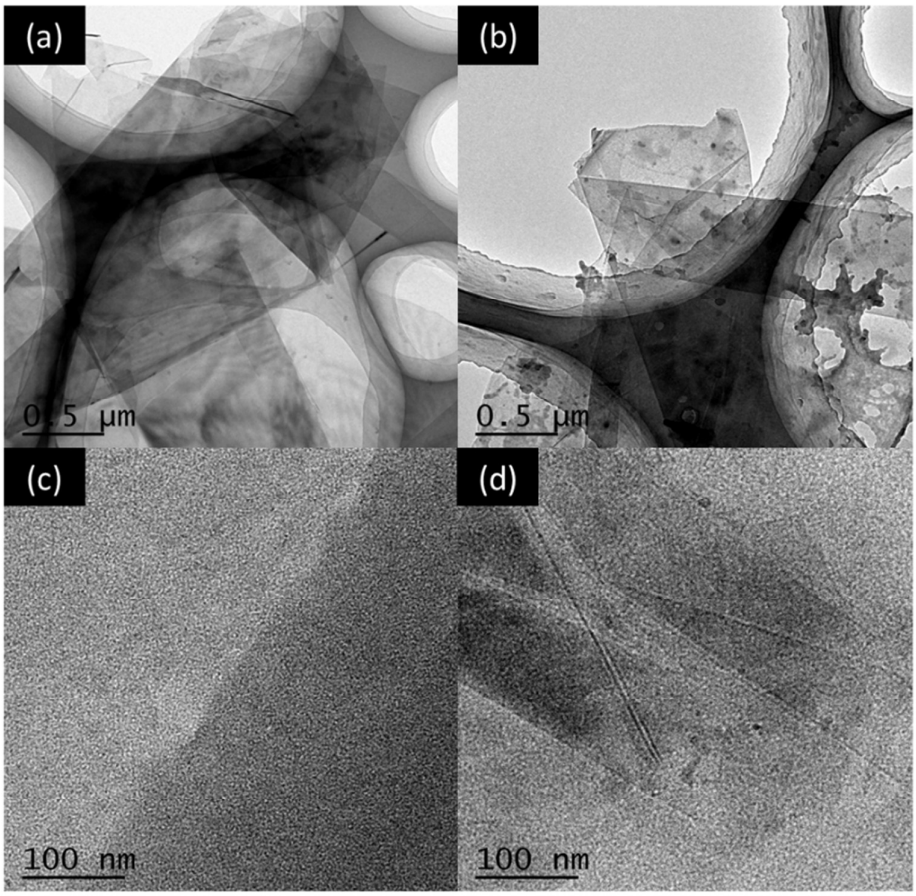

Fig. 5 TEM images of G (a), FG (b), pure PU (c) and FG/PU (d)

AFM and SEM were performed to investigate the surface topography of textured wafers and textured FG/PU composite coatings with different geometrical parameters. As shown in **Fig. 6(a, b and c)**, three-dimension (3D) AFM image and height profile of textured wafers showed that the surface topography consisted of several regular circular cone. The diameter and height of each circular cone were estimated to be 8 and 2 μm. And the distance between adjacent circular cones was 8, 6 and 4μm, respectively. In addition, it could be found from **Fig. 6(d, e and f)** that 8 μm diameter circular cone constituted textured surface, and they were 8, 6 and 4 μm apart, respectively. All the diameter and height of the formed cones were exactly the same. The above geometrical parameters were consistent with the AFM results, which illustrated that the textured surfaces of FG/PU composite coatings were successfully replicated by replication method.

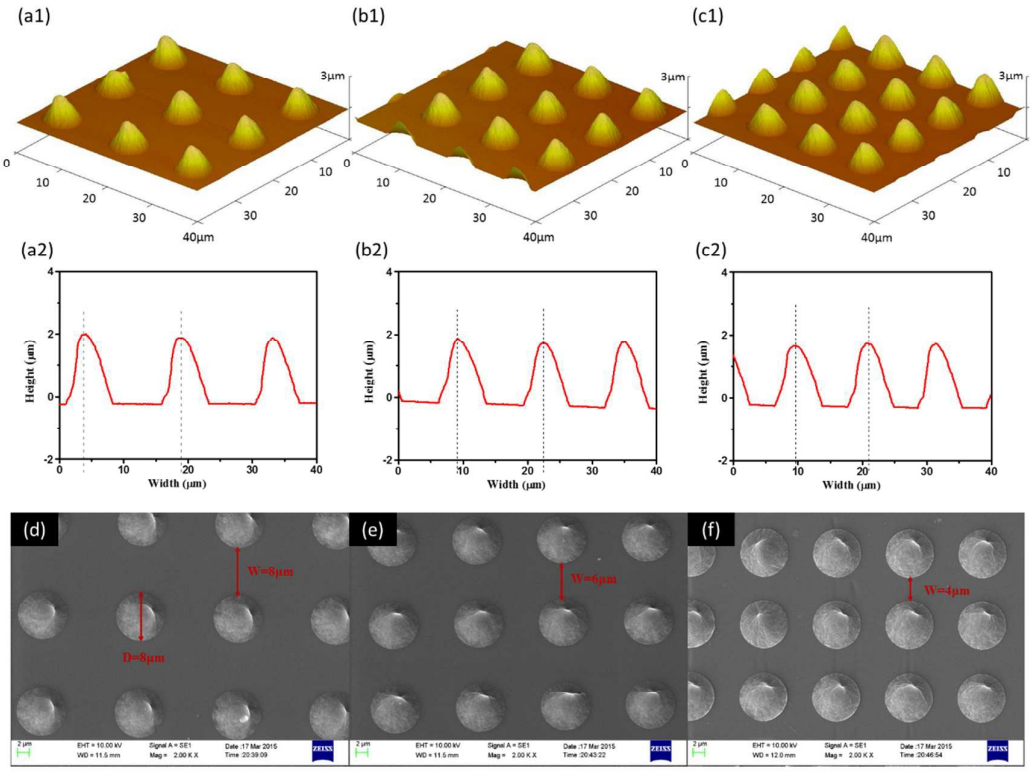

Fig. 6 3D AFM images and height profiles of textured wafers and SEM images of textured FG/PU composite coatings with different geometrical parameters: circular cone with a diameter of 8 μm spaced 8 (a, d), 6 (b, e) and 4 (c, f) μm apart

3.3. Wetting properties

Contact angle tests were conducted to investigate the surface hydrophobicity of PU and FG/PU coatings. A summary of the advancing (θ_a), sessile (θ_s), receding (θ_r) water contact angles (WCA) and contact angle hysteresis (CAH=$\theta_a - \theta_r$) values for all of the samples are listed in **Table 1**. As presented in **Table 1** and **Fig. 7**, θ_a, θ_s and θ_r of smooth PU coating was measured to be about 89.7±2.8°, 82.2±1.5° and 68.9±1.6°. Meanwhile, corresponding to the textured surfaces with circular cone spaced 8, 6 and 4 μm apart, the θ_s values were 87.2±1.2°, 92.3±0.4° and 94.6±2.0°, respectively. And the variation tendency of θ_a and θ_r value was in good agreement with that of θ_s. In other words, a further relevant increase in the contact angle was observed in the PU coatings with textured morphologies. And the WCA increased with decreasing the distance between the circular cones. When it came to FG/PU composite coatings, it presented similar variation tendency. Corresponding to smooth surface and the textured surfaces

with circular cone spaced 8, 6 and 4 μm apart, the θ_s values were 88.4±2.1°, 94.2±1.7°, 98.2±1.2° and 103.4±0.8°, respectively. It is worth noting that the WCAs of FG/PU composite coatings were generally larger than those of PU coatings, which was ascribed to the hydrophobicity of G and the enhancement of roughness resulted from G. Apart from that, the CAH values were calculated between 16 and 21°. Meanwhile, there were no obvious difference for PU and FG/PU coatings with different textured surfaces.

Table 1 The advancing, sessile, receding water contact angles and contact angle hysteresis values for all of the samples

Samples	θ_a	θ_s	θ_r	CAH
PU (smooth)	89.7±2.8°	82.2±1.5°	68.9±1.6°	20.8±4.4°
PU (8μm)	90.0±0.9°	87.2±1.2°	72.9±1.6°	17.1±1.6°
PU (6μm)	97.9±1.1°	92.3±0.4°	78.0±2.6°	19.8±2.4°
PU (4μm)	98.7±1.2°	94.6±2.0°	81.9±1.1°	16.8±2.2°
FG/ PU (smooth)	93.1±2.8°	88.4±2.1°	76.1±4.0°	17.1±2.3°
FG/PU (8μm)	99.1±2.7°	94.2±1.7°	80.7±5.3°	18.4±3.0°
FG/PU (6μm)	103.9±1.6°	98.2±1.2°	86.0±1.8°	17.9±0.9°
FG/PU (4μm)	110.0±0.8°	103.4±0.8°	92.0±3.8°	18.0±3.2°

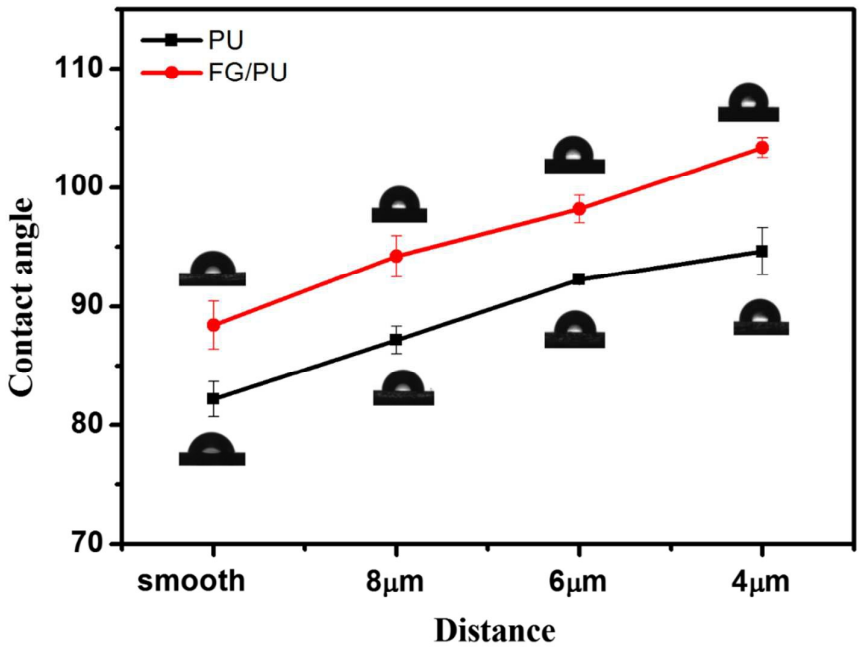

Fig. 7 Sessile water contact angle of PU and FG/PU coatings with different textured surfaces

It is generally believed that a higher contact angle value denotes a more hydrophobic surface[46]. The above results indicate that the surface hydrophobic property depends on not only the textured surface, but also the presence of G. The enhancement of hydrophobic property will be conducive to prevent the absorption of water through the coating[2]. What's more, the influence of textured surface on WCA can be theoretically explained according to the Wenzel and Cassie models. The microstructure can change the solid-liquid interface and weaken the wettability of the textured coatings. Meanwhile, the solid-liquid interface tuned into the composite interface of the air–liquid and solid–liquid interfaces owing to air trapping in the textures[47].

3.4. Anti-corrosion properties

Electrochemical measurements have been widely used to evaluate the corrosion protection behaviour of coatings. The tafel polarization curves of bare substrate, PU and FG/PU coated samples in a corrosive medium (3.5 wt.% NaCl solution) are presented in **Fig. 8(a and b)**. Some corrosion parameters such as current density (I_{corr}), corrosion potential (E_{corr}) and protection efficiency (η) evaluated from the polarization curves for all of the samples are summarized in **Table 2**.

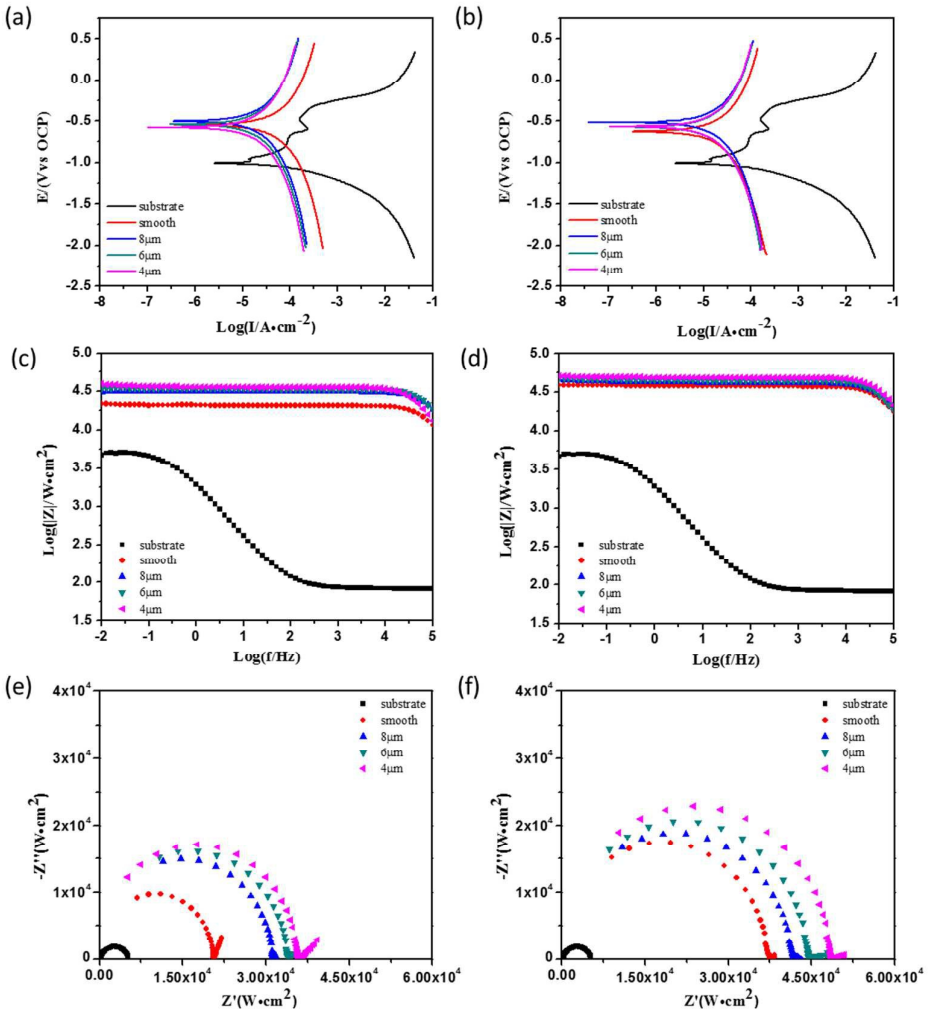

Fig. 8 Tafel polarization curves (a), Bode plots (c) and Nyquist plots (e) of bare substrate, PU coated substrate; Tafel polarization curves (b), Bode plots (d) and Nyquist plots (f) of bare substrate, FG/PU coated substrate

Table 2 Electrochemical parameters for bare and coated substrate obtained from polarization curves

Samples	I_{corr} (Acm^{-2})	E_{corr} (V)	η(%)
substrate	2.126×10^{-5}	-1.0043	
PU (smooth)	4.432×10^{-6}	-0.5475	79.15
PU (8μm)	2.420×10^{-6}	-0.5026	88.62
PU (6μm)	2.097×10^{-6}	-0.5293	90.14
PU (4μm)	1.894×10^{-6}	-0.5796	91.09

FG/ PU (smooth)	2.038×10^{-6}	-0.6274	90.41
FG/PU (8μm)	1.840×10^{-6}	-0.5194	91.34
FG/PU (6μm)	1.641×10^{-6}	-0.5705	92.28
FG/PU (4μm)	1.463×10^{-6}	-0.5700	93.12

The value of η, was calculated from the above value of I_{corr}, according to the following equation (**Equation (1)**) [22, 48]:

$$\eta = \frac{I_{corr}^{\circ} - I_{corr}}{I_{corr}^{\circ}} \times 100\% \quad (1)$$

where, I_{corr}° and I_{corr}, derived from the intersection of the cathodic curves and linear portions of the anodic, are the corrosion current density of bare and coated substrate, respectively.

In general, a lower I_{corr} value and a higher η value indicate a better anti-corrosion property. As shown in **Table 2**, the I_{corr} value presented an order of bare substrate > PU (smooth) > PU (8μm) > PU (6μm) > PU (4μm) and the similar sequence of bare substrate > FG/PU (smooth) > FG/PU (8μm) > FG/PU (6μm) > FG/PU (4μm). By comparing the above results from different angles, five meaningful information can be derived as follows. Firstly, it is evident that the I_{corr} value of coated substrate decreased greatly compared to that of bare substrate. This suggested that organic protective coating could protect materials against corrosion. Secondly, the η value of the textured coating coated substrate was found to be more positive than that of the smooth coating coated substrate, which implied that a hydrophobic coating may indeed reduce the susceptibility of substrate to corrosion. Thirdly, as the distance between the circular cones decreased, the η value of textured coating coated substrate increased accordingly. This point further proofed the importance of textured surface to corrosion resistant. Forthly, the FG/PU coated substrate displayed more positive η value compared with PU coated substrate, which is attributed to the barrier effect of FG. Lastly, the FG/PU coated substrate with the highest texture density displayed the best anti-corrosion performance, which demonstrated that synergistic effect of texture and filler was of great importance.

In addition, electrochemical impedance spectroscopy (EIS) was used to examine the dielectric properties of a medium. Meanwhile, as a kind of effective means, EIS was also applied to evaluate the activity difference between the substrate upon PU and FG/PU coating with different texture density treatment[3, 34]. Presented in **Fig. 8(c and d)** and **Fig. 8(e and f)** are the

Bode plots and Nyquist plots for all measured samples. In general, the value of impedance modulus at the lowest frequency in Bode plots (impedance vs. frequency), and the value of semicircle diameter in Nyquist plots, are proportional to corrosion resistance[49].

Furthermore, to further analyze the EIS results and explore the mechanisms of the corrosive processes, the equivalent circuits in **Fig. 9** were used to fit Nyquist plots by ZSimpWin software[50, 51]. The equivalent circuits are made of resistors, insulators, capacitors, or any of their combination[22]. Nyquist plots of bare substrate exhibited one time-constant, which were appropriate for equivalent circuit of R(QR) shown in **Fig. 9(a)**. When it came to coated substrates, their Nyquist plots showed an extra time-constant due to the coating layer. In consequence, they are fitted using equivalent electrical circuit of R(QR)(QR) presented in **Fig. 9(b)**, which usually described that the electrolyte homogeneously diffuses into coatings causing uniformly distributed reaction sites at interface. As it turned out, the selected equivalent circuits fitted well to Nyquist plots of all samples. And the corresponding electrochemical model impedance parameters derived from outcomes of model fitting are summarized in **Table 3**. Chief among these parameters was R_{film}, which represents the resistance of coating. It is often consider as an indicator of anti-corrosion property.

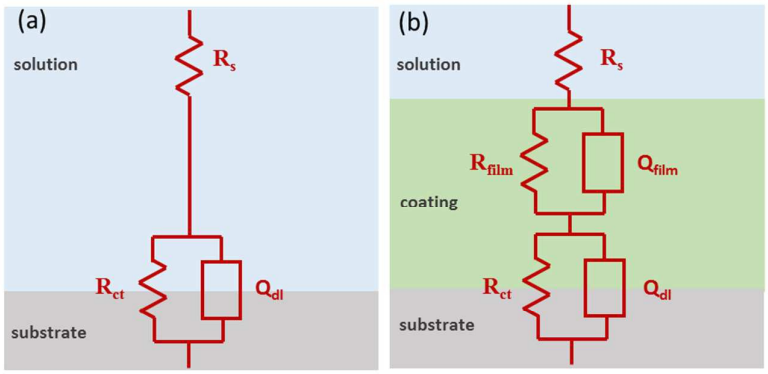

$$Z = R_S + \frac{1}{Q_{dl} + R_{ct}} \qquad Z = R_S + \frac{1}{Q_{film} + R_{film}} + \frac{1}{Q_{dl} + R_{ct}}$$

R_s : solution resistance
Q_{dl} : capacitance of metal/solution interface
R_{ct} : charger chansfer resistance
Q_{film} : capacitance of coating
R_{film} : resistance of coating

Fig. 9 Equivalent circuit for EIS data fitting

Table 3 Electrochemical model impedance parameters from EIS data fitting of PU coatings (a) and FG/PU coatings (b)

(a)

Electrode	substrate	PU (smooth)	PU (8μm)	PU (6μm)	PU (4μm)
$R_s/\Omega\cdot cm^2$	82.1	9.97×10^{-8}	9.999×10^{-8}	5.034×10^{-3}	1.476×10^{-13}
$Q_{film}/F\cdot cm^2$		1.749×10-^{10}	1.076×10^{-10}	1.132×10^{-10}	1.505×10^{-10}
n_{film}		0.9665	0.9657	0.9639	0.9775
$R_{film}/\Omega\cdot cm^2$		2.062×10^{4}	3.135×10^{4}	3.415×10^{4}	3.577×10^{4}
$Q_{dl}/F\cdot cm^2$	1.05×10^{-4}	2.153×10-^{3}	8.947×10^{-3}	2.824	8.963×10^{-4}
n_{dl}	0.8	0.7321	0.8965	4.854×10^{-31}	0.4973
$R_{ct}/\Omega\cdot cm^2$	5287	3.515×10^{9}	9.749×10^{9}	3.273×10^{-2}	2.946×10^{4}
Equivalent circuit	R(QR)	R(QR)(QR)	R(QR)(QR)	R(QR)(QR)	R(QR)(QR)

(b)

Electrode	substrate	FG/PU (smooth)	FG/PU (8μm)	FG/PU (6μm)	FG/PU (4μm)
$R_s/\Omega\cdot cm^2$	82.1	9.985×10^{-8}	9.997×10^{-8}	1×10^{-7}	1.001×10^{-7}
$Q_{film}/F\cdot cm^2$		1.306×10^{-10}	1.584×10^{-10}	1.368×10^{-10}	1.056×10^{-10}
n_{film}		0.9622	0.9359	0.9571	0.9641
$R_{film}/\Omega\cdot cm^2$		3.71×10^{4}	4.176×10^{4}	4.442×10^{4}	4.857×10^{4}
$Q_{dl}/F\cdot cm^2$	1.05×10^{-4}	4.78×10^{-4}	1.558×10^{-4}	3.722×10^{-4}	1.061×10^{-3}
n_{dl}	0.8	0.2265	0.6016	0.4138	0.4897
$R_{ct}/\Omega\cdot cm^2$	5287	2179	2193	4839	3229
Equivalent circuit	R(QR)	R(QR)(QR)	R(QR)(QR)	R(QR)(QR)	R(QR)(QR)

As previously referred to, the value of impedance modulus at the lowest frequency in Bode plots, the value of semicircle diameter in Nyquist plots and the R_{film} are three key indicators to analyze the anti-corrosion performance from EIS measurements. It can be observed obviously that all the three value presented an order of bare substrate < PU (smooth) < PU (8μm) < PU (6μm) < PU (4μm) and the similar sequence of bare substrate < FG/PU (smooth) < FG/PU (8μm) < FG/PU (6μm) < FG/PU (4μm). Besides, it is worth noting that the all the three value of FG/PU composite coatings were generally larger than those of PU coatings. The variation tendency of them was in good agreement with previous results from polarization curve measurements.

Based on above reported literature, the schematic shown in **Fig. 10** was drawn to intuitively

describe the anti-corrosion mechanism of FG reinforced PU nanocomposite coatings with regular texture. The excellent anti-corrosion performance of textured FG/PU composite coating largely depends on two aspects. From the outside, the textured surface can prevent the wetting between etchant solution and coated substrate surface, and sequentially reduce the actual contact area between them[52]. From the interior, the presence of well-dispersed FG in the PU matrix provide a barrier action to diffusion, at the same time reduced the wettability[4].

In addition, the spread of the corrosive medium can be divided into two processes. In the first stage, before water permeation through the coating, the surface hydrophobic property resulted from the texture and FG, is in favour of preventing the absorption of water through the coating. Generally, water serves as a medium for the diffusion of corrosion factors. Preventing water from being absorbed by the coating is equal to preventing the corrosion factors from diffusing through the coating, which can decrease to some extent the rate of diffusion of corrosive factors to the metal-polymer interface. As mentioned before, the enhancement of hydrophobic property will be conducive to prevent the absorption of water. Therefore, the hydrophobic property of coating is relevant to its prevention from corrosion attack. In addition, the solid-liquid interface will turn into the composite interface of the air-liquid and solid-liquid interfaces owing to air trapping in the textures, which reduce contact between water and the surface. Due to the very low diffusion coefficient of water though air, it takes more time for water to diffuse through air layer[2]. In the second stage, during water permeation through the textured FG/PU composite coating, dispersed FG in the PU matrix can increase the tortuosity of corrosive medium diffusion pathway due to its barrier effect[53, 54]. To sum up, the presence of surface texture and FG results in the hydrophobicity and barrier effect of textured FG/PU composite coating, which reduces the contact and interaction between water and surfaces, and increases the tortuosity of corrosive medium diffusion pathway.

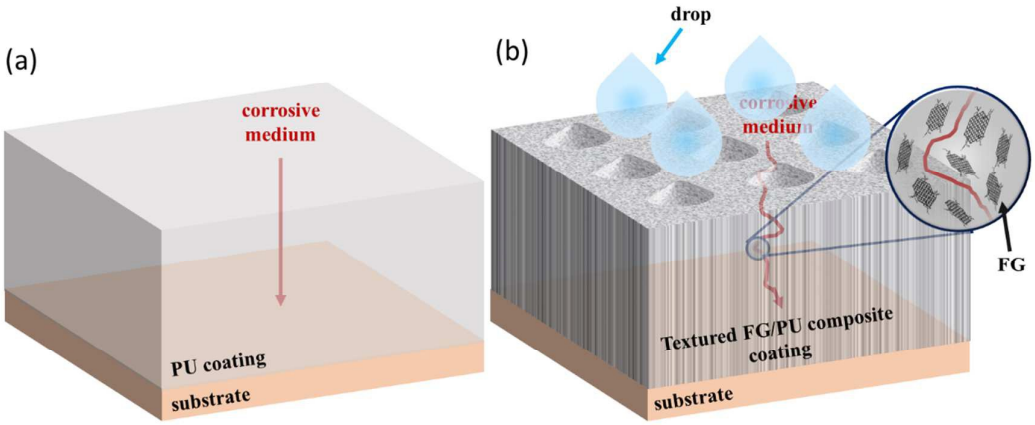

Fig. 10. Schematic of pure PU (a), textured FG/PU composite coating (b) during corrosion process

4. Conclusions

A series of FG reinforced PU nanocomposite coatings with regular texture as corrosion inhibitor were fabricated using replication method. After chemical modification, FG was dispersed homogeneously in the PU matrix. The morphology of the obtained coatings showed circular cone with a diameter of 8 μm spaced 8, 6 and 4 μm apart, respectively. The superior anti-corrosion property of textured FG/PU composite coating is attributed to the presence of surface texture and well-dispersed FG in the PU matrix. The hydrophobicity and barrier effect significantly slow the kinetics of the corrosion process. This paper offers a method for more research and development as well as utilize the synergistic effect of nanofiller and textured surface.

Acknowledgements

The project was supported by the National Key Basic Research Program of China (973) (2014CB643305), National Natural Science Foundation of China (51202263, 51335010) , Ningbo Key Technology Project on Graphene (2013B6013), Zhejiang Province Public Welfare Program (2014C31154) and the Municipal Nature Science Foundation (2014A610132). Thanks for professor zhaoping liu and professor xufeng zhou providing the raw materials of graphene.

References

1. B. P. Singh, B. K. Jena, S. Bhattacharjee and L. Besra, *Surface & Coatings Technology*, 2013, **232**, 475-481.

2. A. C. C. de Leon, R. B. Pernites and R. C. Advincula, *ACS applied materials & interfaces*, 2012, **4**, 3169-3176.

3. K. C. Chang, M. H. Hsu, H. I. Lu, M. C. Lai, P. J. Liu, C. H. Hsu, W. F. Ji, T. L. Chuang, Y. Wei, J. M. Yeh and W. R. Liu, *Carbon*, 2014, **66**, 144-153.

4. L. Calabrese, L. Bonaccorsi, A. Capri and E. Proverbio, *Journal of Coatings Technology and Research*, 2014, **11**, 883-898.

5. Z. S. Petrović and J. Ferguson, *Progress in Polymer Science*, 1991, **16**, 695-836.

6. M. C. L. de Oliveira, R. A. Antunes and I. Costa, *International Journal of Electrochemical Science*, 2013, **8**, 4679-4689.

7. S. Dutta and N. Karak, *Polymer International*, 2006, **55**, 49-56.

8. A. K. Mishra, S. Allauddin, K. R. Radhika, R. Narayan and K. Raju, *Polymers for Advanced Technologies*, 2011, **22**, 882-890.

9. P. L. Li, H. Ren, F. X. Qiu, J. C. Xu, Z. P. Yu, P. F. Yang, B. B. Xu, Y. Jiang and D. Y. Yang, *Polymer-Plastics Technology and Engineering*, 2014, **53**, 1408-1416.

10. B. Yu, X. Wang, W. Y. Xing, H. Y. Yang, L. Song and Y. Hu, *Industrial & Engineering Chemistry Research*, 2012, **51**, 14629-14636.

11. K. Yao, M. Song, D. Hourston and D. Luo, *Polymer*, 2002, **43**, 1017-1020.

12. J. N. Gavgani, H. Adelnia and M. M. Gudarzi, *Journal of Materials Science*, 2014, **49**, 243-254.

13. M. J. Allen, V. C. Tung and R. B. Kaner, *Chemical reviews*, 2009, **110**, 132-145.

14. D. R. Dreyer, R. S. Ruoff and C. W. Bielawski, *Angewandte Chemie International Edition*, 2010, **49**, 9336-9344.

15. A. K. Geim and K. S. Novoselov, *Nature materials*, 2007, **6**, 183-191.

16. K. P. Loh, Q. Bao, P. K. Ang and J. Yang, *Journal of Materials Chemistry*, 2010, **20**, 2277-2289.

17. C. e. N. e. R. Rao, A. e. K. Sood, K. e. S. Subrahmanyam and A. Govindaraj, *Angewandte Chemie International Edition*, 2009, **48**, 7752-7777.

18. W. S. Ma, L. Wu, D. Q. Zhang and S. F. Wang, *Colloid and Polymer Science*, 2013, **291**, 2765-2773.

19. H. K. He and C. Gao, *ACS applied materials & interfaces*, 2010, **2**, 3201-3210.

20. H. J. Song and N. Li, *Applied Physics a-Materials Science & Processing*, 2011, **105**, 827-832.

21. C. H. Chang, T. C. Huang, C. W. Peng, T. C. Yeh, H. I. Lu, W. I. Hung, C. J. Weng, T. I. Yang and J. M. Yeh, *Carbon*, 2012, **50**, 5044-5051.

22. K. C. Chang, C. H. Hsu, H. I. Lu, W. F. Ji, C. H. Chang, W. Y. Li, T. L. Chuang, J. M. Yeh, W. R. Liu and M. H. Tsai, *Express Polymer Letters*, 2014, **8**, 243-255.

23. J. S. Lin, L. W. Wang and G. H. Chen, *Tribology Letters*, 2011, **41**, 209-215.

24. S. Choudhary, H. P. Mungse and O. P. Khatri, *Journal of Materials Chemistry*, 2012, **22**, 21032-21039.

25. S. P. Economopoulos, G. Rotas, Y. Miyata, H. Shinohara and N. Tagmatarchis, *ACS nano*, 2010, **4**, 7499-7507.

26. L.-H. Liu, M. M. Lerner and M. Yan, *Nano letters*, 2010, **10**, 3754-3756.

27. Q. Yang, X. Pan, F. Huang and K. Li, *The Journal of Physical Chemistry C*, 2010, **114**, 3811-3816.

28. X. Qi, K. Y. Pu, H. Li, X. Zhou, S. Wu, Q. L. Fan, B. Liu, F. Boey, W. Huang and H. Zhang, *Angewandte Chemie International Edition*, 2010, **49**, 9426-9429.

29. Y. Xu, H. Bai, G. Lu, C. Li and G. Shi, *Journal of the American Chemical Society*, 2008, **130**, 5856-5857.

30. L. Q. Xu, L. Wang, B. Zhang, C. H. Lim, Y. Chen, K.-G. Neoh, E.-T. Kang and G. D. Fu, *Polymer*, 2011, **52**, 2376-2383.

31. S. K. Yadav, Y. C. Jung, J. H. Kim, Y. I. Ko, H. J. Ryu, M. K. Yadav, Y. A. Kim and J. W. Cho, *Particle & Particle Systems Characterization*, 2013, **30**, 721-727.

32. X. Wang, W. Xing, L. Song, B. Yu, Y. Hu and G. H. Yeoh, *Reactive and Functional Polymers*, 2013, **73**, 854-858.

33. B. Yu, X. Wang, W. Xing, H. Yang, X. Wang, L. Song, Y. Hu and S. Lo, *Chemical Engineering Journal*, 2013, **228**, 318-326.

34. K. C. Chang, W. F. Ji, M. C. Lai, Y. R. Hsiao, C. H. Hsu, T. L. Chuang, Y. Wei, J. M. Yeh and W. R. Liu, *Polymer Chemistry*, 2014, **5**, 1049-1056.

35. W. Zhao, L. Wang and Q. Xue, *The Journal of Physical Chemistry C*, 2010, **114**, 11509-11514.

36. L. Calabrese, L. Bonaccorsi, A. Capri and E. Proverbio, *Progress in Organic Coatings*, 2014, **77**, 1341-1350.

37. M. Fir, B. Orel, A. S. Vuk, A. Vilcnik, R. Jese and V. Francetic, *Langmuir*, 2007, **23**, 5505-5514.

38. W. Zhao, J. Pu, Q. Yu, Z. Zeng, X. Wu and Q. Xue, *Colloids and Surfaces A: Physicochemical and Engineering Aspects*, 2013, **428**, 70-78.

39. Y. J. Kim and B. K. Kim, *Colloid and Polymer Science*, 2014, **292**, 51-58.

40. X. Wang, W. Y. Xing, L. Song, H. Y. Yang, Y. Hu and G. H. Yeoh, *Surface & Coatings Technology*, 2012, **206**, 4778-4784.

41. A. Kausar, S. Zulfiqar and M. I. Sarwar, *Polymer Degradation and Stability*, 2013, **98**, 368-376.

42. T. L. Wang and F. J. Huang, *Polymer international*, 1998, **46**, 280-284.

43. J. M. Hu, X. Jia, C. H. Li, Z. Y. Ma, G. X. Zhang, W. B. Sheng, X. L. Zhang and Z. Wei, *Journal of Materials Science*, 2014, **49**, 2943-2951.

44. C. A. Bauer, T. V. Timofeeva, T. B. Settersten, B. D. Patterson, V. H. Liu, B. A. Simmons and M. D. Allendorf, *Journal of the American Chemical Society*, 2007, **129**, 7136-7144.

45. X. J. Shen, X. Q. Pei, S. Y. Fu and K. Friedrich, *Polymer*, 2013, **54**, 1234-1242.

46. C. L. Zhou, X. Lu, Z. Xin, J. Liu and Y. F. Zhang, *Progress in Organic Coatings*, 2013, **76**, 1178-1183.

47. z. chen, W. Zhao, J. Xu, M. Mo, s. peng, Z. Zeng, x. Wu and q. Xue, *RSC Adv.*, 2015, DOI: 10.1039/c5ra04658k.

48. S. Banerjee, A. Mishra, M. M. Singh, B. Maiti, B. Ray and P. Maiti, *Rsc Advances*, 2011, **1**, 199-210.

49. X. J. Cui, X. Z. Lin, C. H. Liu, R. S. Yang, X. W. Zheng and M. Gong, *Corrosion Science*, 2015, **90**, 402-412.

50. L. B. Boinovich, S. V. Gnedenkov, D. A. Alpysbaeva, V. S. Egorkin, A. M. Emelyanenko, S. L. Sinebryukhov and A. K. Zaretskaya, *Corrosion Science*, 2012, **55**, 238-245.

51. G. X. Shen, Y. C. Chen, L. Lin, C. J. Lin and D. Scantlebury, *Electrochimica Acta*, 2005, **50**, 5083-5089.

52. Y. Liu, S. Y. Li, J. J. Zhang, J. A. Liu, Z. W. Han and L. Q. Ren, *Corrosion Science*, 2015, **94**, 190-196.

53. M. Mo, W. Zhao, Z. Chen, Q. Yu, Z. Zeng, X. Wu and Q. Xue, *RSC Adv.*, 2015, **5**, 56486-56497.

54. K. C. Chang, W. F. Ji, C. W. Li, C. H. Chang, Y. Y. Peng, J. M. Yeh and W. R. Liu, *Express Polymer Letters*, 2014, **8**, 908-919.

Graphical Abstract

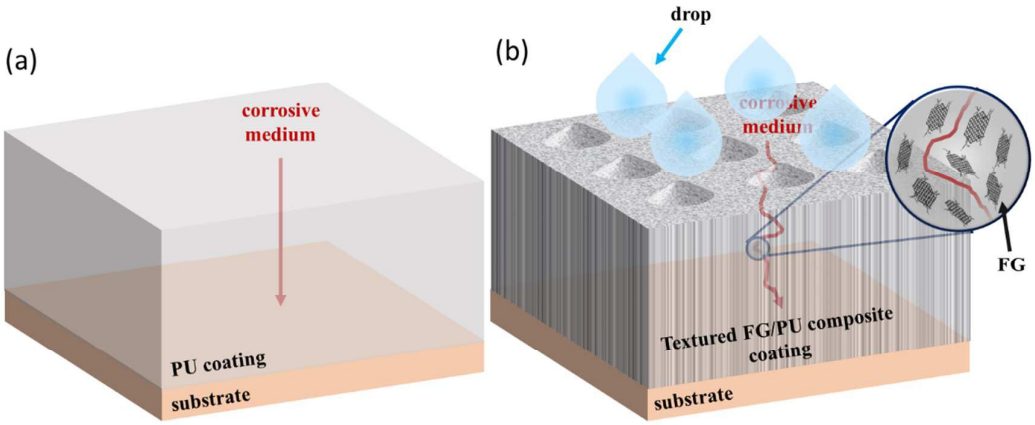

The schematic was drawn to intuitively describe the anti-corrosion mechanism of functional graphene reinforced polyurethane nanocomposite coatings with regular texture.